General Disclaimer

One or more of the Following Statements may affect this Documer

- This document has been reproduced from the best copy furnished by the organizational source. It is being released in the interest of making availabl much information as possible.

- This document may contain data, which exceeds the sheet parameters. It w furnished in this condition by the organizational source and is the best copy available.

- This document may contain tone-on-tone or color graphs, charts and/or pic which have been reproduced in black and white.

- This document is paginated as submitted by the original source.

- Portions of this document are not fully legible due to the historical nature of of the material. However, it is the best reproduction available from the origi submission.

X-620-69-35
PREPRINT

NASA TM X-63464

THE INFRARED INTERFEROMETER SPECTROMETER EXPERIMENT FOR THE MARS MARINER '71 ORBITAL MISSION

FEBRUARY 1969

GSFC

GODDARD SPACE FLIGHT CENTER
GREENBELT, MARYLAND

X-620-69-35
PREPRINT

HE INFRARED INTERFEROMETER SPECTROMETER EXPERIMENT

FOR THE MARS MARINER '71 ORBITAL MISSION

R. A. Hanel, B. J. Conrath, W. A. Hovis, V. Kunde,
P. D. Lowman, C. Prabhakara, B. Schlachman
Goddard Space Flight Center
Greenbelt, Maryland

G. V. Levin
Biospherics Research, Inc.
Washington, D. C.

February 1969

GODDARD SPACE FLIGHT CENTER
Greenbelt, Maryland

THE INFRARED INTERFEROMETER SPECTROMETER EXPERIMENT FOR THE MARS MARINER '71 ORBITAL MISSION

R. A. Hanel, B. J. Conrath, W. A. Hovis, V. Kunde,
P. D. Lowman, C. Prabhakara, B. Schlachman
Goddard Space Flight Center
Greenbelt, Maryland

G. V. Levin
Biospherics Research, Inc.
Washington, D. C.

ABSTRACT

The infrared interferometer spectrometer to be carried on the Mars Mariner '71 mission is essentially a Michelson type interferometer operating in the spectral range 200-1600 cm^{-1}, with an apodized spectral resolution corresponding to 2.4 cm^{-1}. Use of the instrument on a Mars orbiting spacecraft provides an opportunity for inferring spatial and temporal behavior of various physical parameters associated with the planetary atmosphere and surface. Included among these parameters are atmospheric and surface temperatures and total atmospheric water vapor content. A search can be made for minor atmospheric constituents which are optically active in the spectral range of the observations. Information on the types of surface materials present can be obtained from the phenomenon of reststrahlen, and analyses of cooling curves should also be useful in surface studies. To illustrate the information content of the interferometer measurements, examples of synthetic spectra calculated using model atmospheres are given. Techniques for obtaining the various physical parameters from measured spectra are discussed. Preliminary analysis indicates that water vapor amounts as low as 0.1 precipitable microns should be detectable under reasonable assumptions on the behavior of the atmospheric temperature profile. The inferred parameters should provide essential input for studies of the physical behavior of the atmosphere, such as the nature of the general circulation. Of considerable biological interest are the possible implications of the measurements on the existence or nonexistence of water in the liquid phase. The identification of surface materials and of minor atmospheric constituents may also contribute to biological studies.

PRECEDING PAGE BLANK NOT FILMED.

CONTENTS

ILLUSTRATIONS

ILLUSTRATIONS (Continued)

TABLES

THE INFRARED INTERFEROMETER SPECTROMETER EXPERIMENT FOR THE MARS MARINER '71 ORBITAL MISSION

I. INTRODUCTION

The thermal emission spectrum of a planet depends on many atmospheric and surface parameters. The most important atmospheric parameters are the types of optically active gases present, abundance and distribution of these gases and the temperature profile, while the most important surface parameters are temperature, pressure, composition, and structure.

The infrared interferometer spectrometer (IRIS "M") experiment for the Mariner '71 orbital mission is designed to provide spectral measurements of the thermal emission spectrum of the Martian surface and atmosphere. The spectral range covered is 200 - 1600 cm^{-1} with 2.4 cm^{-1} wide spectral resolution elements. Spatial resolution is approximately 126 km for an altitude of 1600 km. The orbital mission allows the Martian atmospheric and surface properties to be studied with respect to geographic location and time variation.

Absorption features due to polyatomic molecules lie within the measured spectral range. To date only CO_2 (Owen, 1966; Spinrad, Schorn, Moore, Giver, and Smith, 1966; Belton, Broadfoot, and Hunten, 1968; Giver, Inn, Miller, and Boese, 1968), H_2O (Kaplan, Munch, and Spinrad, 1964; Schorn, Spinrad, Moore, Smith, and Giver, 1967) and CO (Connes, 1968) have been positively identified by spectroscopic means in the Martian atmosphere. A tentative identification of O_2 has been made by Belton and Hunten (1968) from two weak absorption lines of the oxygen A band. Analysis of these lines yields a O_2 abundance of 20 cm-atm or less. The strongly absorbing spectral region centered near 667 cm^{-1} due to carbon dioxide will provide information on the vertical temperature distribution in the atmosphere while the more nearly transparent portions of the spectrum will be well suited for the search for minor atmospheric constituents and for the possible observation of reststrahlen phenomena caused by minerals composing the Martian surface.

The scientific objectives of the experiment will first be discussed, including the inference of temperature profiles, estimation of water vapor content, detection of minor atmospheric constituents, and the identification of reststrahlen features associated with surface materials. The use of these parameters in obtaining a better understanding of the physics of the Martian atmosphere, the composition and structure of the surface, and possible biological implications will be considered. Finally, a discussion of the instrumentation will be given, along with examples of data acquired with early versions of the instrumentation in the laboratory and from a balloon in the earth's atmosphere.

II. SCIENTIFIC OBJECTIVES

The basic scientific objectives of the experiment are to utilize measurements of the spectral radiance $I(\nu)$ of the thermally emitted radiation from the Martian atmosphere and surface to infer atmospheric and surface parameters. These parameters will then be employed in studies of the physical behavior of the atmosphere, investigations of the surface composition and structure, and biological studies.

In order to obtain some feeling for the quantities to which such measurements are sensitive, it is instructive to consider the theoretical expression for $I(\nu)$ which can be written

$$I(\nu) = \epsilon(\nu)\, B(\nu, T_s)\, \tau_s(\nu) - \int_{\log P_t}^{\log P_s} B\left[\nu, T(\log P)\right] \frac{\partial \tau(\nu, \log P)}{\partial \log P}\, d \log P \qquad (1)$$

$B(\nu,T)$ is the Planck intensity at wave number ν and temperature T, and the transmittance for the atmospheric gas between pressure level P and the effective top of the atmosphere P_t is represented by $\tau(\nu, \log P)$. The subscript s refers to surface values, and $\epsilon(\nu)$ represents the emissivity of the planetary surface. The atmosphere has been assumed to be in local thermodynamic equilibrium, and the small contribution to $I(\nu)$ from radiation reflected from the surface has been neglected. The first term in (1) represents the thermal emission from the surface, attenuated by the atmosphere, and is dependent on the surface emissivity and surface temperature as well as the total atmospheric transmittance. The second term represents the atmospheric emission and is dependent on the atmospheric temperature profile through the source function $B[\nu, T(\log P)]$ and on the type, total amount, and vertical distribution of the optically active gases through the transmittance $\tau(\nu, \log P)$.

Techniques for inferring the various physical parameters from measurements of $I(\nu)$ and their applications to surface, atmospheric, and biological studies are considered below.

1. Atmosphere

To illustrate the information contained in the type of measurements anticipated from the experiment, several synthetic spectra have been calculated using (1) and assuming model Martian atmospheres. Figure 1 shows the results of such calculations for the spectral region in the vicinity of the 667 cm^{-1} absorption band of CO_2. For this illustration, a temperature profile based on

calculations of radiative and convective equilibrium by Gierasch and Goody (1968) was employed. The profile, which is for equinox conditions at the equator at 1600 hours local time, possesses a "discontinuity" of 36°K across a 10 meter thick boundary layer at the surface. Since the Gierasch-Goody calculations extend only to 30 km, the temperature profile was extrapolated isothermally above that level. A surface pressure of 5 mb was employed, and the chemical composition was taken as essentially pure CO_2 (68 m-atm). The surface emissivity $\epsilon(\nu)$ was set equal to unity for all ν in this case.

In calculating the values of $\tau(\nu, \log P)$ required in (1), the monochromatic molecular absorption coefficient along the atmospheric slant path was determined by summing the contribution of all individual lines at a particular frequency using theoretically calculated line positions and strengths. The spectral integration techniques employed have been described previously (Kunde, 1968 a,b). The theoretical molecular line parameters for the 667 cm^{-1} carbon dioxide band were obtained from Drayson and Young (1967). The effect of a triangular instrument function of 2 cm^{-1} total width at half maximum was included. Figure 1 shows the resulting synthetic spectra expressed in terms of the brightness temperatures corresponding to the calculated radiances. Spectra corresponding to the contributions of the various isotopic species are shown as well as the complete spectrum including all isotopes. The isotopes were weighted by their relative terrestrial abundances. The lower and upper vibrational states for each vibrational band are also denoted, and the integrated intensity of each $^{12}C\ ^{16}O_2$ band, relative to the $00^00 \rightarrow 01^10$ band, is given in parentheses after the vibrational transition.

The Q branches of the fundamental and strong combination bands are evident in the spectra as is the rotational structure of some of the bands. For identification purposes the observed spectra will exhibit even more line structure than shown in Figure 1 as the unapodized spectra expected from the instrument correspond to a higher spectral resolution of 1.2 cm^{-1}. Qualitatively the general shape of the temperature profile in the region of the $^{12}C\ ^{16}O_2$ Q branch (667 cm^{-1}) absorption can be determined by observing the shape of the Q branch in the spectrum. Contributions to the radiances in the strongly absorbing Q branch come from relatively high in the atmosphere. On Earth most of the absorption and subsequent re-emission occurs in the stratosphere where the temperature is increasing with altitude, resulting in a higher brightness temperature for the Q branch region with respect to the adjacent portion of the spectrum. For the Mars model, contributions from the higher portions of the atmosphere correspond to cooler temperatures and the minimum brightness temperature occurs in the Q branch region. Thus the 667 cm^{-1} Q branch qualitatively indicates whether the temperature is increasing or decreasing in the region of Q branch absorption.

To obtain quantitative information on the temperature profile throughout the atmosphere, more complex considerations are required. A considerable literature exists on computational techniques for obtaining temperature profiles from remote radiometric measurements (Wark, 1961; Yamamoto, 1961; Twomey, 1963; 1965; King, 1964; Wark and Flemming, 1966; Conrath, 1968). The principle of obtaining temperature profiles from observed spectra can be understood by considering the atmospheric term in (1). The factor $|\partial\tau(\nu, \log P)/\partial \log P|$ can be regarded as the weight given the source function $B[\nu, T(\log P)]$ at each level P. Figure 2 shows weighting functions for several different wavenumbers calculated using the model atmosphere discussed above. Because the principal levels of contribution move from higher to lower levels in the atmosphere in moving from the opaque band center to the less opaque band wings, measurements across an absorption band permit a reconstruction of the temperature profile. Considerable overlap of the weighting functions causes solutions obtained for the temperature profile to be sensitive to instrumental noise, and considerable effort has been expended in developing techniques which will provide stability by introducing smoothing constraints into the solutions.

Temperature profiles have been successfully recovered from data obtained for the Earth's atmosphere during balloon flights. An example of data from a balloon flight with a breadboard version of an early IRIS instrument covering the spectral range 500 to 2000 cm^{-1} with spectral resolution elements 5 cm^{-1} wide is shown in Figure 3. The temperature profile inferred from these data (Conrath, 1968) is shown in Figure 4 along with radiosonde data taken at a nearby station for comparison. Computational techniques developed for application to data from the Earth's atmosphere are adaptable to the Martian case in a general sense although considerable work is necessary for the specific application.

In order to properly interpret the observed spectrum and to obtain the correct temperature profile, it is necessary to have accurate values of the carbon dioxide mixing ratio and the surface pressure. The curve-of-growth techniques utilized in the near-infrared cannot be applied to the thermal emission spectra directly due to the additional complication of the source function. The possibility of employing differential pressure effects in the 667 cm^{-1} CO_2 band as a means for estimating the surface pressure and CO_2 mixing ratio is currently being investigated. Should this approach prove to be unfeasible, ground-based values or values derived from the occultation experiment will be used. It will, of course, be possible to check these values, along with the other inferred atmospheric parameters, for internal consistency by comparison of a synthetic spectrum with the observed one.

Among the possible minor atmospheric constituents, water vapor is of primary interest because of its biological as well as geological importance. In order to obtain an estimate for the sensitivity of the anticipated spectral

measurements to the total water vapor content in an atmospheric column, synthetic spectra have been calculated for the region of rotational water vapor absorption between 200 cm^{-1} and 600 cm^{-1}. The same atmospheric temperature profile was used as in the calculations of the CO_2 spectra described previously, and a constant water vapor mixing ratio was assumed. The positions and strengths of the rotational water vapor lines were obtained from Benedict (private communication), and spectral resolution elements 2 cm^{-1} wide were again employed. Figure 5a shows the resulting brightness temperature spectra for total water vapor contents of 14.6 precipitable microns and for 0.1 precipitable micron. For the 0.1 precipitable micron water vapor content, the brightness temperature fluctuation is approximately 1°K which corresponds to a radiance fluctuation of 4.5×10^{-8} watt cm^{-1} $ster^{-1}$. The noise level of the IRIS "M" instrument is expected to be of that order so 0.1 precipitable micron of water vapor represents a signal corresponding to the noise level. The detectability can be improved by averaging several spectra together.

The sensitivity of the measurements to total water vapor content depends on the behavior of the atmospheric temperature relative to the surface temperature. The rotational H_2O spectrum was also computed without the 36°K boundary layer "discontinuity" with the results shown in Figure 5b. The changes in brightness temperature due to the presence of 0.1 precipitable micron of water vapor are approximately 0.5°K. Removal of the temperature "discontinuity" therefore decreases the apparent strength of the water vapor absorption features only by a factor of approximately two.

In addition to water vapor, the presence of other minor atmospheric constituents is of interest since their presence reflects on the evolution of the atmosphere and may also be indicative of biological activity. The various possible minor constituents on Mars for which upper abundance limits have been determined are listed in Table 1. In most cases, the upper limits were deduced from the absence of absorption lines or bands in the observed spectra. The search for minor constituents, such as those listed in Table 1, must be based in part on a compilation and study of laboratory spectra of the gases involved. In addition, systematic procedures must be developed for predicting abundances in a self-consistent fashion from thermodynamic, chemical, and photochemical equilibrium considerations. Several recent investigations illustrate the type of procedure required even though some of their results are now out-dated. Considering thermodynamic and photochemical equilibrium for nitrogen oxides on Mars—along with the upper limits for O_2 and NO—Sagan, Hanst, and Young (1965) have theoretically reduced the upper limit for the abundance of NO_2 below its previously observed value. Lippincott, Eck, Dayhoff and Sagan (1967) reduced the equilibrium upper limit of NO_2 several orders of magnitude below the value of Sagan et al. In their investigation, Lippincott et al. included a larger number of

Table 1
Upper Limits on Abundances for Possible Minor Constituents
in the Martian Atmosphere

Molecule	Path Length (cm atm)	Reference
O_3	0.004	e
NO	20	b
NO_2	0.0008	c
N_2O	0.08	b
HNO_2	0.16	d
HCHO	0.3	b
COS	0.2	b
H_2S	7.5	b
CH_4	0.1	b
C_2H_4	3	a
C_2H_6	1	a
NH_3	0.1	b

a) Kuiper, G. P., in Atmospheres of the Earth and Planets (Ed. G. P. Kuiper). Chapter 12. University of Chicago Press, Chicago, 1952.

b) Kuiper, G. P., Comm. of the Lunar and Planetary Laboratory, 2, No. 31, 79, 1964.

c) Marshall, J. V., Comm. of the Lunar and Planetary Laboratory, 2, No. 35, 167, 1964.

d) Sagan, C., Hanst, P. L., and A. T. Young, Planet. Space Sci., 13, 73, 1965

e) Belton, M. J. S., and D. M. Hunten, Ap. J., 153, 963, 1968

equilibrium reactions than Sagan et al. but considered only chemical equilibrium. The initial CO_2 mixing ratio used by Lippincott et al. was 0.10 which is considerably lower than current best estimates so their results can no longer be considered quantitatively valid. Bortner and Alyea (1968) have calculated the steady state concentrations of eighteen species as a function of altitude in the Martian atmosphere. Investigations of the type mentioned above are valuable as a guide in the search for minor constituents and they should be extended to include as many chemical reactions as possible.

In most cases, the concentrations of minor constituents can be expected to be sufficiently small so that it will be difficult to directly recognize the spectral features of the gases in the measurements. In these cases, techniques will have to be utilized for improving the effective signal-to-noise ratio such as averaging a number of spectra together and using cross-correlation analysis. In the latter approach, the cross-correlation $c(\nu)$ is formed between the known spectrum of the gas to be identified $T(\nu)$ and the measured brightness temperature spectrum $\tilde{T}(\nu)$

$$c(\nu) = \int T(\nu') \, \tilde{T}(\nu + \nu') \, d\nu' \qquad (2)$$

A significant peaking of $c(\nu)$ at zero lag would be indicative of the presence of the gas in question.

One example of the possible uses of the parameters derivable from the thermal emission spectra is a study of the Martian general circulation. The lack of appreciable amounts of water vapor and bodies of liquid water will tend to simplify the general circulation of Mars compared to Earth. On the other hand, the possible freezing of CO_2 at the winter pole (Leighton and Murray, 1966) may complicate the flow patterns. An investigation of the Martian circulation may be made with numerical models (e.g. Leovy and Mintz, 1966) or analytical techniques (Gierasch and Goody, 1968). Studies of the general circulation and possible correlations with the wave of darkening, inquiries into the composition of the polar caps, and other branches of investigation using the data anticipated from this instrument are being pursued.

2. Surface

For studies of the Martian surface, it is necessary to choose spectral intervals where the atmosphere is nearly transparent so the first term in (1) is dominant. Such atmospheric "windows" exist in the 8-13μ region and in some portions of the region from 18 to 50μ (Kunde, 1967). If the surface emissivity

$\epsilon(\nu)$ possesses distinct features in these spectral intervals, then it may be possible to identify the type of material present.

The phenomenon of reststrahlen in some minerals produces variations in $\epsilon(\nu)$ within the appropriate spectral intervals. This phenomenon was first noticed by optical physicists in the reflectance spectra of polished crystalline minerals such as quartz, salt, and corundum. The marked increase of reflectance in certain wavelengths longer than 8 microns was used to localize the areas of the spectrum where the reststrahlen bands occurred. Recently, this optical phenomenon has been revived for remote sensing. Measurements by several investigators (Hovis and Callahan, 1966; Lyon, 1965) have shown that the reststrahlen of silicate bearing minerals varies in wavenumber with the concentration of the silicate. Igneous rocks are often classified by the SiO_2 content. Granite with more than 65% SiO_2 is considered acidic and dunite with less than 45% SiO_2 ultra basic.

The measured reststrahlen of four typical igneous rocks are shown in Figure 6 for four fractured but unpolished solid samples. As can be seen the peak of the various reststrahlen varies from about 8.5 microns to about 11 microns with the most acidic having the peak at shortest wavelength. Though there is no satisfactory theoretical explanation for this behavior, a large number of measurements have found no exceptions. There is a weakening of the reststrahlen features as the material is ground to smaller sizes as shown in Figure 7. Though the reststrahlen remain they are considerably weaker in the smaller particles and thus require greater instrumental accuracy for detection than is the case for the solid samples.

The investigations of reststrahlen mentioned above were restricted to wave numbers greater than approximately 455 cm^{-1}. The spectroscopic work of Aronson, Emslie, Allen and McLinden (1966) on minerals indicates that considerable information on surface composition can also be obtained from the 50-667 cm^{-1} spectral region.

Cooling curves can provide another means of acquiring information on the nature of the surface materials. Ideally, one would like to obtain the surface temperature at a particular location as a function of local time through a complete day-night cycle. In practice, it will be difficult to get such data for one small surface area, but it should be possible to obtain measurements from various points on relatively homogeneous surface features intersected by the terminator. Computational techniques have been developed for obtaining the parameter $(\rho k c)^{1/2}$ from the cooling curves, where ρ, k, and c are respectively the density, thermal conductivity, and specific heat of the surface material (Wesselink, 1946, Jaeger, 1953).

3. Biological Inferences

Observations of various atmospheric and surface parameters will provide a basis for possible biological inferences. The problem of whether it is physically possible for liquid water to exist at the surface is of primary concern. Therefore, since the surface pressure appears to be in the vicinity of the triple point pressure for water, it is highly important to obtain accurate determinations of the surface temperature as well as the total atmospheric pressure at as many locations as possible. The maximum brightness temperature observed in the high resolution spectra will provide a better estimate for the surface temperature than can generally be obtained from broad band radiometric measurements.

The surface features visible to the IRIS will be compared with the same features as observed by the infrared radiometer, television, and ultraviolet spectrometer for possible correlations. The possibility that large areas of vegetation may provide identifiable spectral features is currently being investigated. If this should prove to be true, comparisons of observed IRIS spectra with a catalog of spectra of interesting terrestrial compounds can be made.

Study of the distribution of atmospheric water vapor should provide some indication of the most likely locations in which biological processes may exist. Observation of other minor atmospheric constituents may also be indicative of biological activity. For example, photosynthesis might be detected through the atmospheric depletion of a gas during the sunlit period and the atmospheric increase of that gas, or another, during the dark period. This and other possible indicators of biological activity are currently being studied.

III. INSTRUMENTATION

The proposed instrument is a Michelson type interferometer which is in all critical areas (detector, beamsplitter, auxiliary interferometer, calibration, and large parts of the electronic circuitry) identical to the interferometer designed for the Nimbus "B" and "D" meteorological satellites. The Nimbus "B" instrument had passed all environmental tests for spacecraft use and would have yielded data from an Earth orbit were it not for a launch malfunction in the Thor booster (May 17, 1968). Some of the mechanical and electrical configurations and circuits, however, will have to be changed for two reasons. First, the interface with the existing Mariner spacecraft and its power and data handling systems will require some modifications to the instrument, and second, the experience gained in extensive testing of the Nimbus instruments suggests several improvements which permit an increase in spectral resolution to become equivalent to 2.4 cm^{-1} in the apodized spectra and to 1.2 cm^{-1} in the unapodized one.

This increase in resolution is considered significant. It will allow the recognition of individual lines in the rotation-vibration bands of CO_2 which are spaced at approximately 1.6 cm^{-1}.

1. The Design

Table 2 summarizes the more important parameters of the Nimbus interferometers and the Mars Mariner '71 instrument (IRIS "M"). Figure 8 shows a simplified diagram of the proposed instrument.

Table 2

Characteristic Parameters of Nimbus and Mariner Interferometers

	IRIS "B"	IRIS "D"	IRIS "M"
Nominal spectral range, cm^{-1}	500-2000	200-1600	200-1600
Number of samples per interferogram	3408	4096	4096
Reference Wave Length, Å	5852	5852	6929 (or 7032)
No. of Reference fringes per sample interval	2	3	3
Optical path difference, cm	0.4	0.72	0.85
Displacement of mirror during interferogram, cm	0.2	0.36	0.427
Velocity of mirror, cm/sec^{-1}	0.0184	0.0275	0.0235
Width of resolved spectral intervals, apodized, (unapodized) cm^{-1}	5 (2.5)	2.8 (1.4)	2.4 (1.2)
Area of aperture, cm^2	13	15	15
Solid angle, ster.	$1.57 \cdot 10^{-2}$	$5.5 \cdot 10^{-3}$	$4.7 \cdot 10^{-3}$

Table 2 (Continued)

	IRIS "B"	IRIS "D"	IRIS "M"
Field of view, degree	~8	~5	~4.5
Duration of interferogram, sec	10.956	13.107	18.2
Basic frame period, sec	16	16	21
Bits in A/D converter	8+Gain	9+Gain	12
Neon reference, frequency, Hz	625	937.5	675
Frequencies in data channel, Hz	18-73	11-88	9.5-75.8
Number of resolved spectral intervals, apodized	300	500	585
Noise equiv. radiance (watt cm^{-1} $ster^{-1}$)	6×10^{-8} *	6×10^{-8} *	3×10^{-8} **
Operating temperature of detector, °K	250	250	250

* Measured value
** Design goal

The essential part of the interferometer is the beamsplitter which divides the incoming radiation into two approximately equal components. After reflection from the fixed and moving mirrors, respectively, the two beams interfere with each other with a phase difference proportional to the optical path difference between both beams. The recombined components are then focused onto the detector where the intensity is recorded as a function of path difference, δ. Since the mirror motion is phase locked to a stable clock frequency, the mirror path difference is also proportional to time. For quasi-monochromatic radiation, a circular fringe pattern appears at the focal plane of the condensing mirror. There the detector size is chosen to cover just the smallest central fringe for the highest wavenumber of interest. This aperture also determines the field of view of the instrument.

The central fringe may be light or dark depending on the path difference between the two beams. For polychromatic radiation and neglecting constant terms, the signal at the detector, called the interferogram. is

$$i(\delta) = \int_0^\infty K_\nu (B_\nu - B_i) \cos (2\pi\nu\delta - \phi_\nu)\, d\nu .$$

The amplitude is proportional to a responsivity factor K_ν and the difference in radiance between the scene within the field of view B_ν, and B_i, the Planck function corresponding to the instrument temperature. The phase is defined with respect to a point chosen as close as possible to, but not necessarily at, the zero path difference point. Imperfect optical compensation and residual phase shift in the analog part of the data channel cause the angle ϕ to depend somewhat on the wavenumber. Reconstruction of the spectrum is performed on the ground by a digital computer.

The cesium Iodide beamsplitter of the Nimbus "D" and Mariner instrument is optically flat to a fraction of a visible fringe. It has a multilayer dielectric coating which is optimized to the 6 - 50μ region except for a small area in the center where the beamsplitter is coated to perform well in the visible and near infrared. In this center region, the fringe control interferometer operates. It utilizes not only the same beamsplitter but also the prime infrared interferometer mirrors. The fringe control interferometer generates a sine wave of 675 Hz at the silicon diode detector from a nearly monochromatic spectral line of a low pressure neon discharge lamp. The line is isolated by an interference filter. The 675 Hz signal serves, after being divided by three, as a sample command and assures equal distance sampling, and secondly, it is compared in phase to a clock frequency to provide the error signal for the phase locked loop.

The Michelson mirror assembly has an electromagnetic drive coil and also a pick up coil to generate a voltage proportional to mirror velocity. The velocity signal is also used in a feedback arrangement to provide electrical damping and to make the system insensitive to moderate levels of external vibration. The phase locked condition of the Michelson mirrcr provides a constant mirror velocity and permits a constant data rate; moreover, the data stream can be synchronized with the spacecraft clock.

The Image Motion Compensation and Calibration system channels radiation from several sources to the interferometer. After 7 interferograms are taken in the operating mode, one is taken from a built-in warm blackbody (290°K) followed by another set of 7 planetary interferograms and finally by an interferogram from the interstellar background (4°K). The spectra from the blackbody and from space serve calibration purposes to be discussed later.

The instrument generates main data and housekeeping data. The main data are quantized in a 12 bit analog to digital converter. Sixty four words of housekeeping information (blackbody temperature, voltages, bore sighted radiometer, etc.) are transmitted just before and also just after each interferogram. The total number of bits per frame is then 50688. One spectrum corresponds, therefore, to about 10 TV lines.

Some of the housekeeping data are multiplied with the main data and are then transmitted just before and just after each interferogram. This set of housekeeping data is required in the data reduction process. Another set of housekeeping data for instrument performance evaluation is transmitted via the spacecraft system.

2. Data Reduction in Ground Based Computer

The data reduction process consists of four steps:

1. A check of consistency and completeness of input tape and processing of housekeeping information.

2. Fourier transformation of all interferograms by the Cooley-Tukey method.

3. Phase correction, and application of calibration procedure.

4. Production of output tapes which contain the calibrated spectra, housekeeping information and orbital parameters.

In the check of consistency and completeness, the total number of words per interferogram is determined. Housekeeping data are converted into engineering units such as temperatures by application of conversion tables established during preflight calibrations.

Spectra which pass the screening procedure mentioned above will then be transformed, corrected in phase, and submitted to the calibration procedure.

3. Calibration

The instrument is exposed occasionally to a built-in calibration blackbody and to outer space, by rotation of the Image Motion Compensation Mirror (IMCC). The calibration spectra are transformed in the same manner as the spectra obtained while viewing Mars. The amplitude c_v in the spectrum is proportional to the difference in radiance between the instrument and the target.

$$c_\nu = r_\nu (B_{target} - B_{instrument})$$

The factor of proportionality is the responsivity of the instrument.

One obtains a set of three equations; one for the target (index 1), one for the cold blackbody (index 2), and one for the warm blackbody (index 3). Under the assumptions that the responsivity, r_ν, is independent of the target brightness and that the detection and amplification is a linear process, the 3 equations may be solved to yield B_1 as well as r_ν and B_i. If one uses the interstellar background as the cold reference (~4°K), then B_2 is for all practical purposes zero and the equations simplify to

$$B_1 = B_3 \frac{C_2 - C_1}{C_2 - C_3},$$

$$r_\nu = \frac{C_2 - C_3}{-B_3}.$$

$$B_i = B_3 \frac{C_2}{C_2 - C_3}$$

The equation for B_1 is used to reduce the spectra. Neither the responsivity nor the instrument temperature are contained explicitly in this equation. The calibration spectra C_2 and C_3 are the average of many individual spectra so that the random effects in these spectra are greatly reduced. Then the sample standard deviation s_ν of the responsivity is determined for each orbit.

$$s_\nu = \left(\frac{\sum_{i=1}^{k} (r_\nu - \bar{r}_\nu)^2}{k - 1} \right)^{1/2}$$

The r_i are the responsivities computed from each calibration pair (hot and cold blackbody). The average responsivity per orbit is called $\bar{r}_\nu$ and k is the number of calibration pairs per orbit. The standard deviation gives the short time repeatability of the instrument and allows a judgement of the magnitude of the random errors in each spectral interval. The noise equivalent radiance may be calculated from

$$NER = \frac{s B_3}{\bar{r}_\nu}$$

A comparison of the mean orbital responsivity for each spectral interval from orbit to orbit, and from day to day yields the long term drift.

The derived instrument temperature T_i which is calculated from B_i and the instrument temperature measured by the thermistors embedded in the housing should be in close agreement. A deviation from this agreement is used as a caution flag which calls for a special investigation if it should occur.

In preparation for space flight the Nimbus IRIS "B" instrument was tested on the spacecraft in a thermal vacuum chamber. The data were stored on the on-board tape recorder and then transmitted via the spacecraft telemetry system. The instrument had reached the operating temperature near 250°K, the reference target simulating outer space was at liquid nitrogen temperatures, and the on-board calibration blackbody was reading about 280°K. A typical interferogram is shown in Figure 9.

The instrument was then exposed to a blackbody of 279°K mounted in front of the earth part. A calibrated spectrum was generated using only a single interferogram from that blackbody and the calibration procedure described above. The calibrated spectrum is shown in Figure 10. Averaging of several spectra, of course, improves the signal-to-noise ratio further.

4. Supporting Measurements

To facilitate better discrimination between dark and bright areas a small radiometer, sensitive between 0.6 and 0.8 micron (Silicon cell) and having the same field of view, as the interferometer is bore-sighted with the interferometer. Data are read out as part of the housekeeping information with each interferogram. Furthermore, correlation of the spectra with data of other experiments, such as TV, or infrared mapping experiments, would be very desirable.

IV. SUMMARY

The infrared interferometer spectrometer experiment will provide information on a wide range of physical parameters associated with the Martian atmosphere and surface. These data can be applied toward an understanding of many problems associated with the planet, such as the general circulation of the atmosphere, structure and composition of the surface, and the possible existence of biological activity. In the present report, it has been possible to give only rather general treatments of a few of the areas to which the experiment is applicable. Effort is currently being devoted to developing in a more quantitative fashion the various techniques required for extracting the desired physical parameters from the type of spectral data anticipated.

REFERENCES

1. Aronson, J. R., Emslie, A. G., Allen, R. V., and H. G. McLinden, "Far Infrared Spectra of Silicate Minerals for Use in Remote Sensing of Lunar and Planetary Surfaces," Final Report, Contract NAS 8-20122 to George C. Marshall Space Flight Center, NASA, April 16, 1966.

2. Belton, M. J. S., Broadfoot, A. L., and D. M. Hunten, "Abundance and Temperature of CO_2 on Mars during the 1967 Opposition," J. Geophys. Res., 73, 4795-4806 (1968).

3. Belton, M. J. S., and D. M. Hunten, "A Search for O_2 on Mars and Venus: A Possible Detection of Oxygen in the Atmospheres of Mars," Ap. J., 153, 963-974 (1968).

4. Connes, P., private communication, 1968.

5. Conrath, B. J., "Inverse Problems in Radiative Transfer: A Review, in Proceedings of the XVIII Astronautical Congress", ed. by Michal Lunc, Pergamon Press, pp. 339-360 (1968).

6. Drayson, R. S., and C. Young, "The Frequencies and Intensities of Carbon Dioxide Absorption Lines Between 12 and 18 Microns," University of Michigan Technical Report 08183-1-T (1967).

7. Gierasch, P. and R. Goody, "A Study of the Thermal and Dynamical Structure of the Martian Lower Atmosphere," Planet. Space Sci., 16, 615-646 (1968).

8. Giver, L. P., Inn, E. C. Y., Miller, J. H., and R. W. Boese, "The Martian CO_2 Abundance from Measurements in the 1.05μ Band," Ap. J., 153, 285-289 (1968).

9. Hovis, W. A., and W. R. Callahan, "Infrared Reflectance of Igneous Rocks, Tuffs and Red Sandstone from 0.5 to 22 Microns," J.O.S.A., 56, 639 (1966).

10. Jaeger, J. C., "Conduction of Heat in a Solid with Periodic Boundary Conditions, with an Application to the Surface Temperature of the Moon," Proc. Cambridge Phil. Soc., 49, 355-359 (1953).

11. Kaplan, L. D., Munch, G., and H. Spinrad, "An Analysis of the Spectrum of Mars," Ap. J., 1-15 (1964).

12. King, J. I. F., "Inversion by Slabs of Varying Thickness," J. of Atmos. Sci., 21, 324-326 (1964).

13. Kunde, V. G., "Theoretical Computations of The Outgoing Infrared Radiance from a Planetary Atmosphere," NASA Technical Note TND-4045 (1967).

14. Kunde, V. G., "Theoretical Molecular Line Absorption of CO in Late-Type Atmospheres," Ap. J., 153, 435-450 (1968a).

15. Kunde, V. G., "Theoretical Molecular Line Absorption of CO in Late Spectral Type Atmospheres," NASA Technical Note TN D-4798 (1968b).

16. Leighton, R. B., and B. C. Murray, "Behavior of Carbon Dioxide and Other Volatiles on Mars," Science, 153, 136-144 (1966).

17. Leovy, C. B., and Y. Mintz, "A Numerical General Circulation Experiment for the Atmosphere of Mars," Rand Corporation Memorandum RM-5110-NASA, Dec. (1966).

18. Lyon, R. J. P., "Analysis of Rocks by Spectral Infrared Emission (8 to 25 Microns)," Economic Geology, 60, 715 (1965).

19. Schorn, R. A., Spinrad, H., Moore, R. C., Smith, H. J., and L. P. Giver, "High-Dispersion Spectroscopic Observations of Mars II. The Water-Vapor Variations," Ap. J., 743-752 (1967).

20. Spinrad, H., Schorn, R. A., Moore, R., Giver, L. P., and H. J. Smith, "High-Dispersion Spectroscopic Observations of Mars I. The CO_2 Content and Surface Pressure," Ap. J., 146, 331-338 (1966).

21. Twomey, S., "On the Numerical Solution of Fredholm Integral Equations of the First Kind by Inversion of the Linear System Produced by Quadrature," Machinery, 10, 97-101 (1963).

22. Twomey, S., "The Application of Numerical Filtering to the Solution of Integral Equations Encountered in Indirect Sensing Measurements," J. of the Franklin Institute, 229, 95-109 (1965).

23. Owen, T., "The Composition and Surface Pressure of the Martian Atmosphere: Results from the 1965 Opposition," Ap. J., 146, 257-270 (1966).

24. Wark, D. Q., "On Indirect Temperature Soundings of the Stratosphere from Satellites," J. Geophys. Res., 60, 77-82 (1961).

25. Wark, D. Q., and H. E. Fleming, "Indirect Measurements of Atmospheric Temperature Profiles from Satellites: I. Introduction," Monthly Weather Review, 94, 351-362 (1966).

26. Wesselink, A. J., "Heat Conductivity and Nature of the Lunar Surface Material," Bull. of the Astronomical Institutes of the Netherlands, 10, 351-363 (1948).

27. Yamamoto, G., "Numerical Method for Estimating the Stratospheric Temperature Distribution from Satellite Measurements in the CO_2 Band," J. of Meteorology, 18, 581-588 (1961).

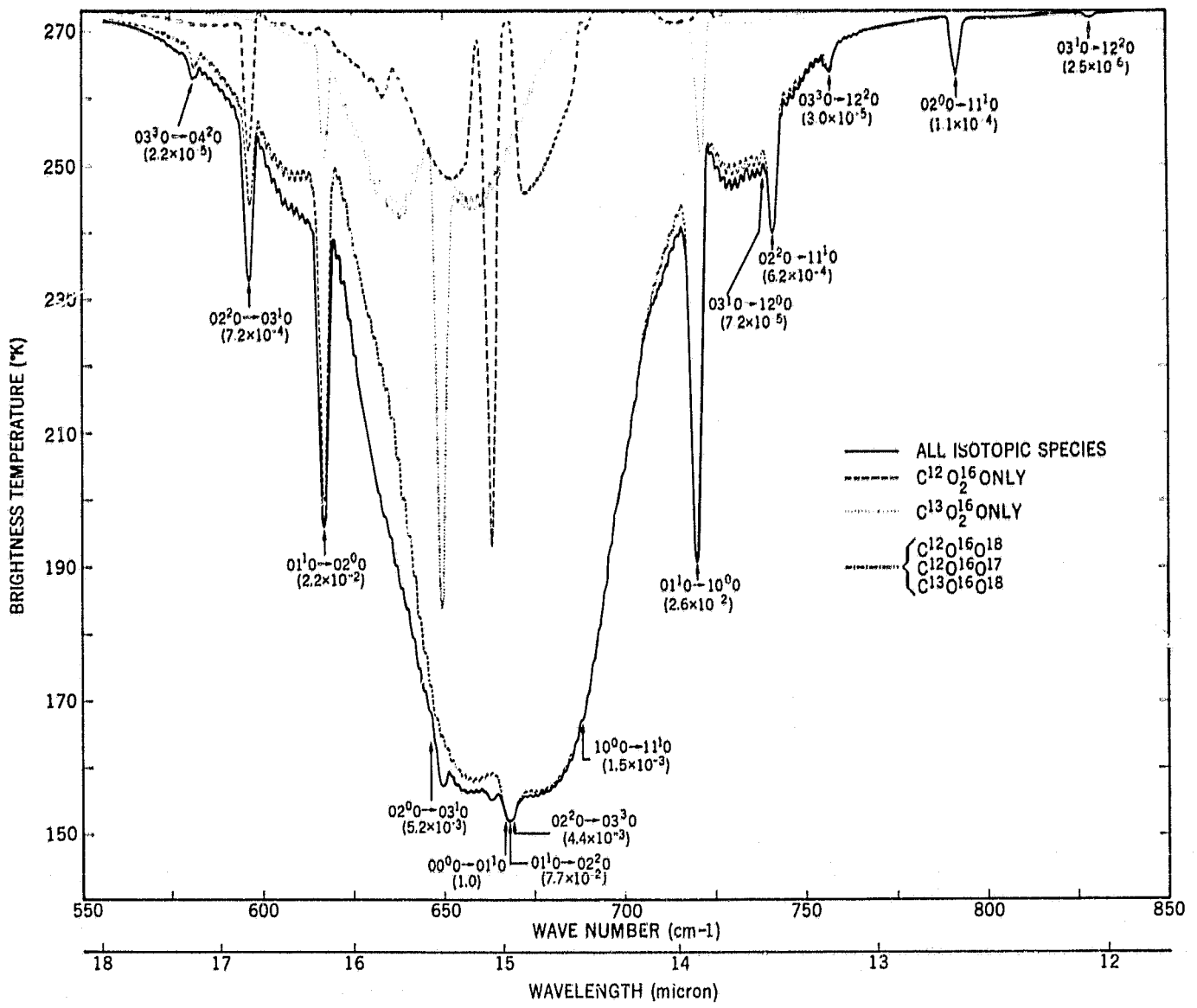

Figure 1. Synthetic brightness temperature spectra for the 667 cm^{-1} CO_2 absorption band. The model atmosphere employed in the calculations is described in the text, and the isotopic species used in each case is shown in the legend.

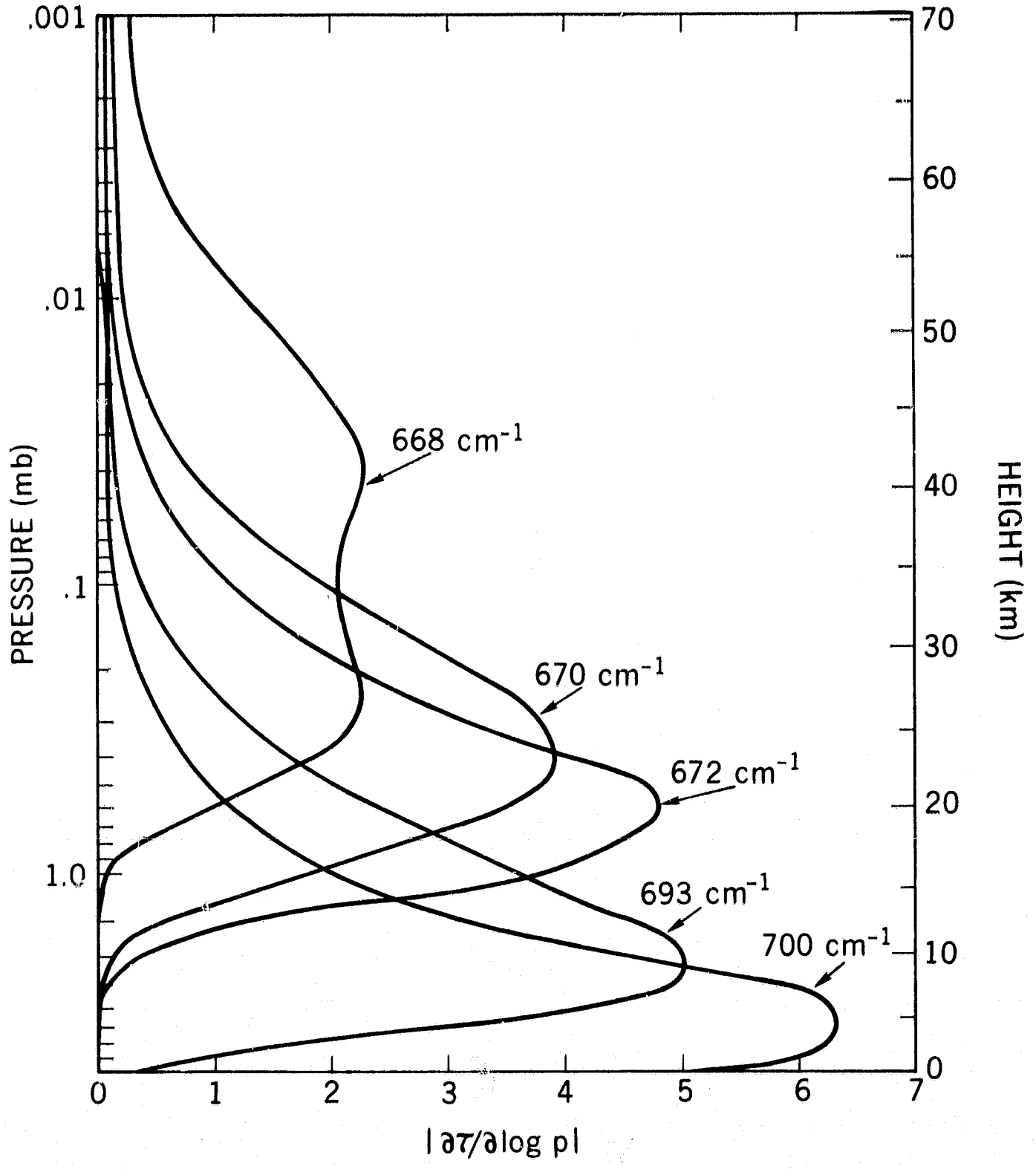

Figure 2. Sample weighting functions for the 667 cm^{-1} carbon dioxide absorption band. An essentially pure CO_2 (68 m-atm) atmosphere with a 5 mb surface pressure was assumed, and spectral resolution elements 2 cm^{-1} wide were employed. The examples shown give an indication of the height range over which information on the temperature profile can be obtained.

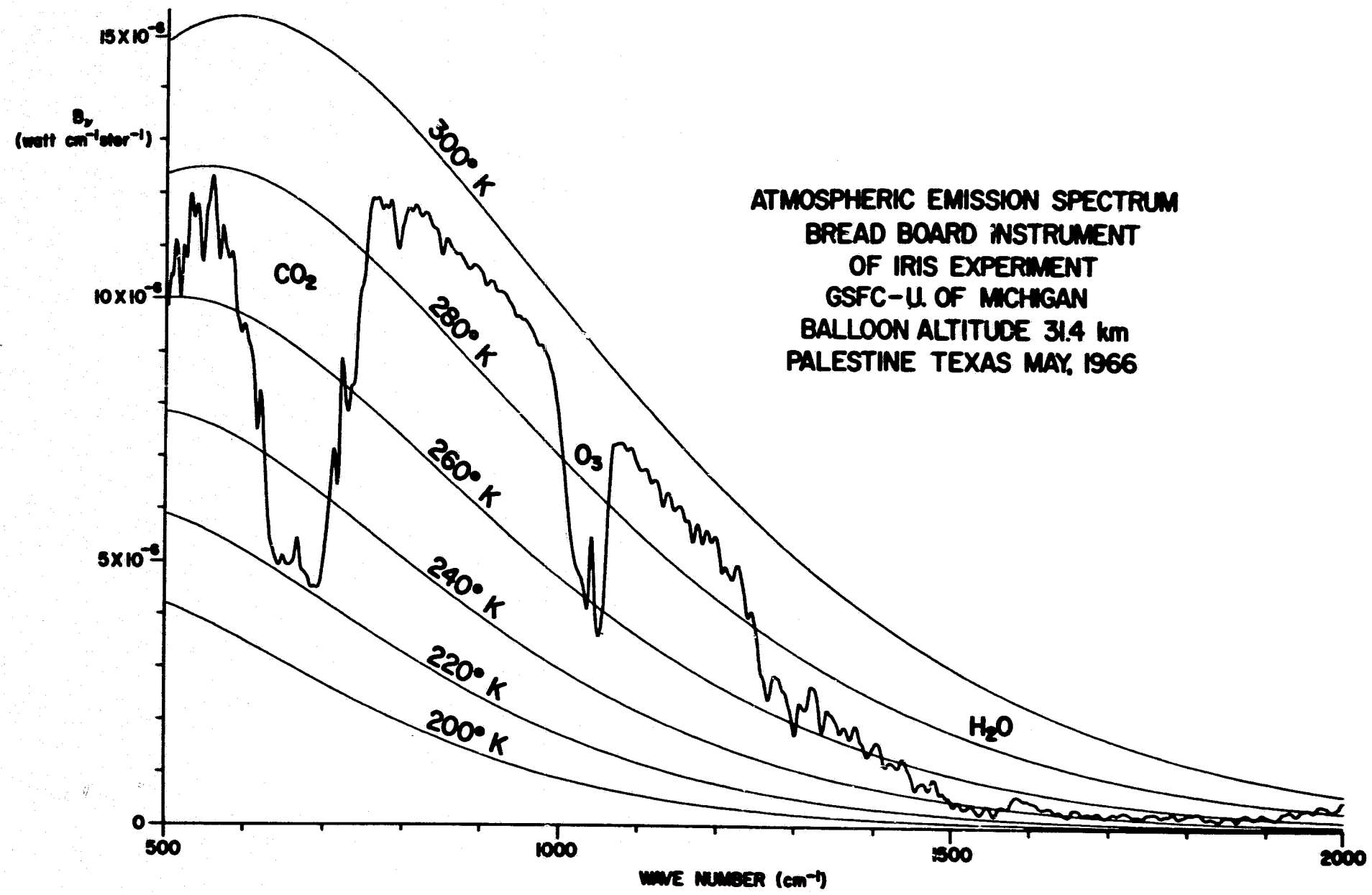

ATMOSPHERIC EMISSION SPECTRUM
BREAD BOARD INSTRUMENT
OF IRIS EXPERIMENT
GSFC–U. OF MICHIGAN
BALLOON ALTITUDE 31.4 km
PALESTINE TEXAS MAY, 1966

Figure 3. Spectrum of the terrestrial atmosphere obtained with an IRIS instrument during a high altitude balloon flight. This version of the instrument covered the spectral range between 500 cm^{-1} and 2000 cm^{-1} with spectral resolution elements 5 cm^{-1} wide.

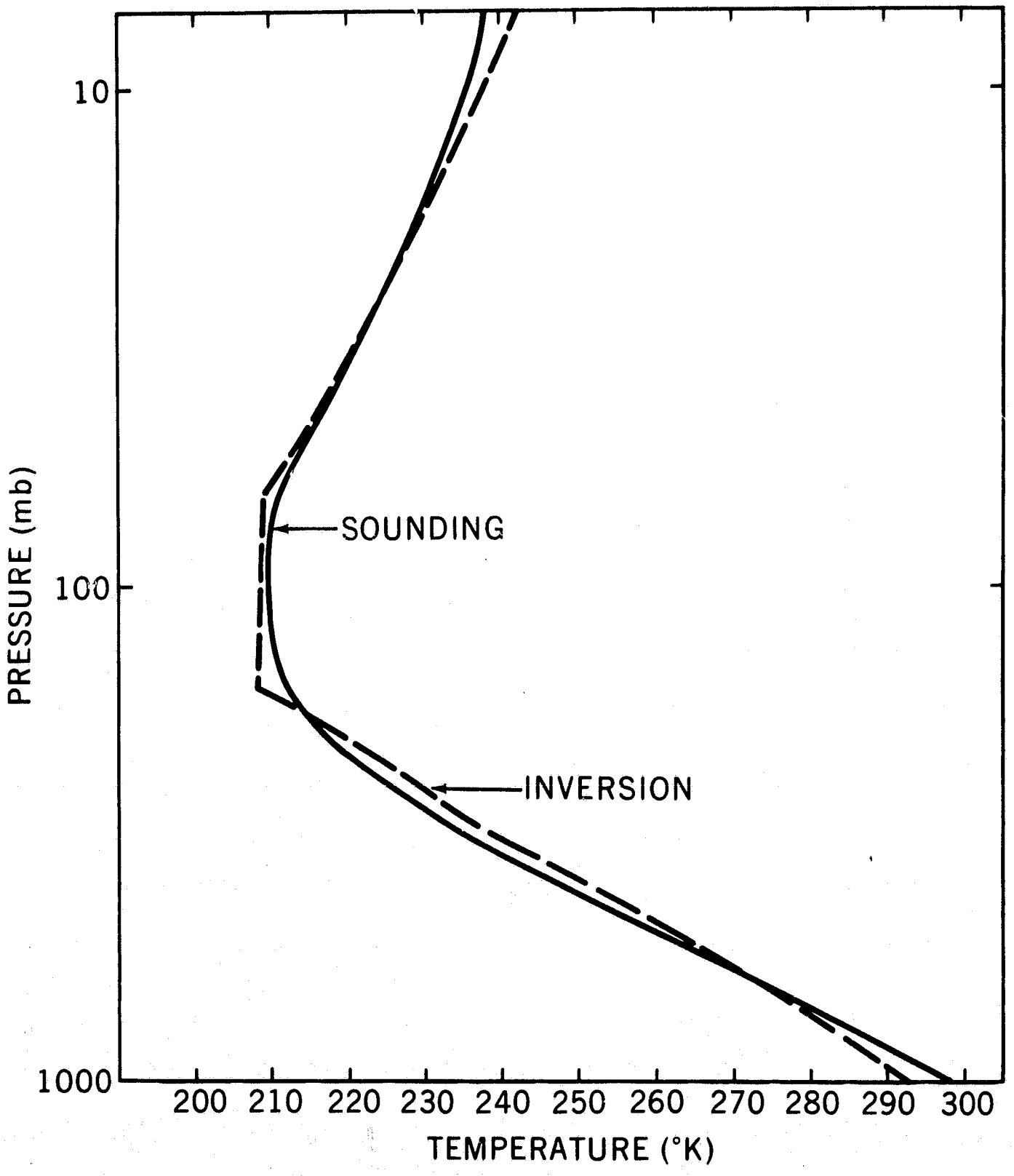

Figure 4. Estimate of the terrestrial temperature profile obtained from the measured spectrum shown in Figure 3. A temperature profile based on data obtained from a nearby radiosonde station is shown for comparison.

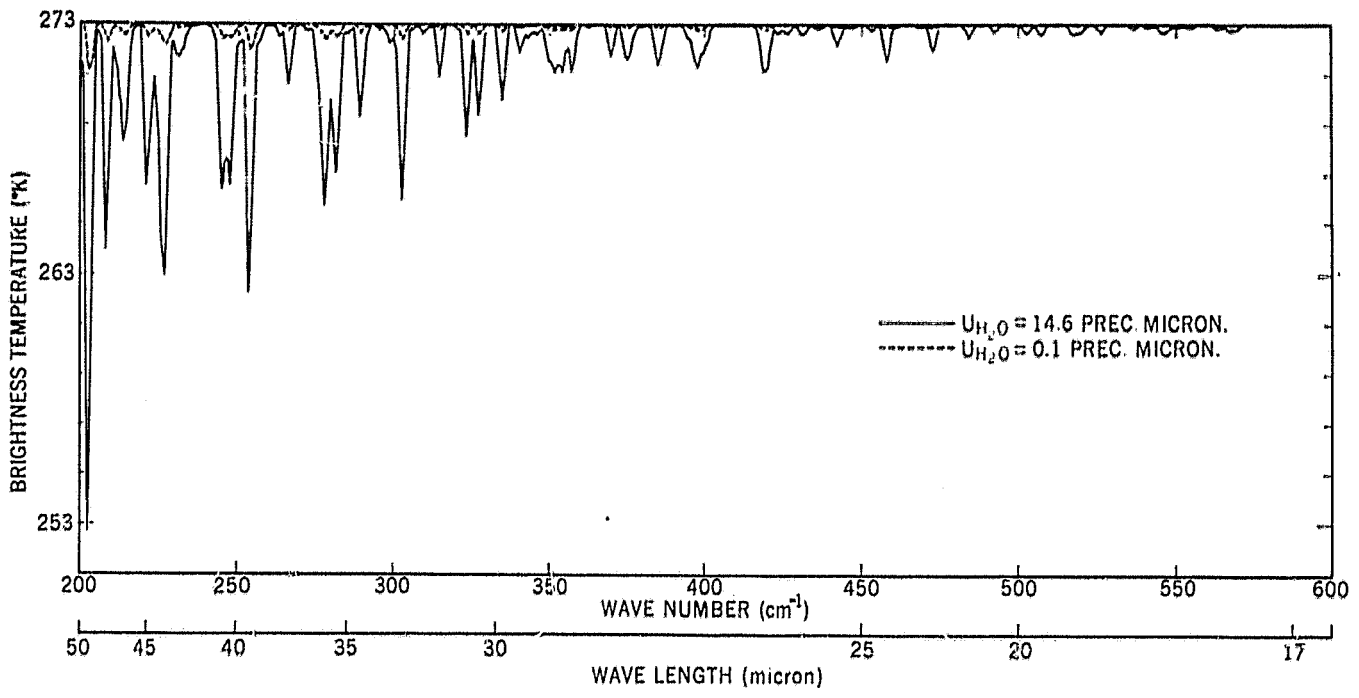

(a)

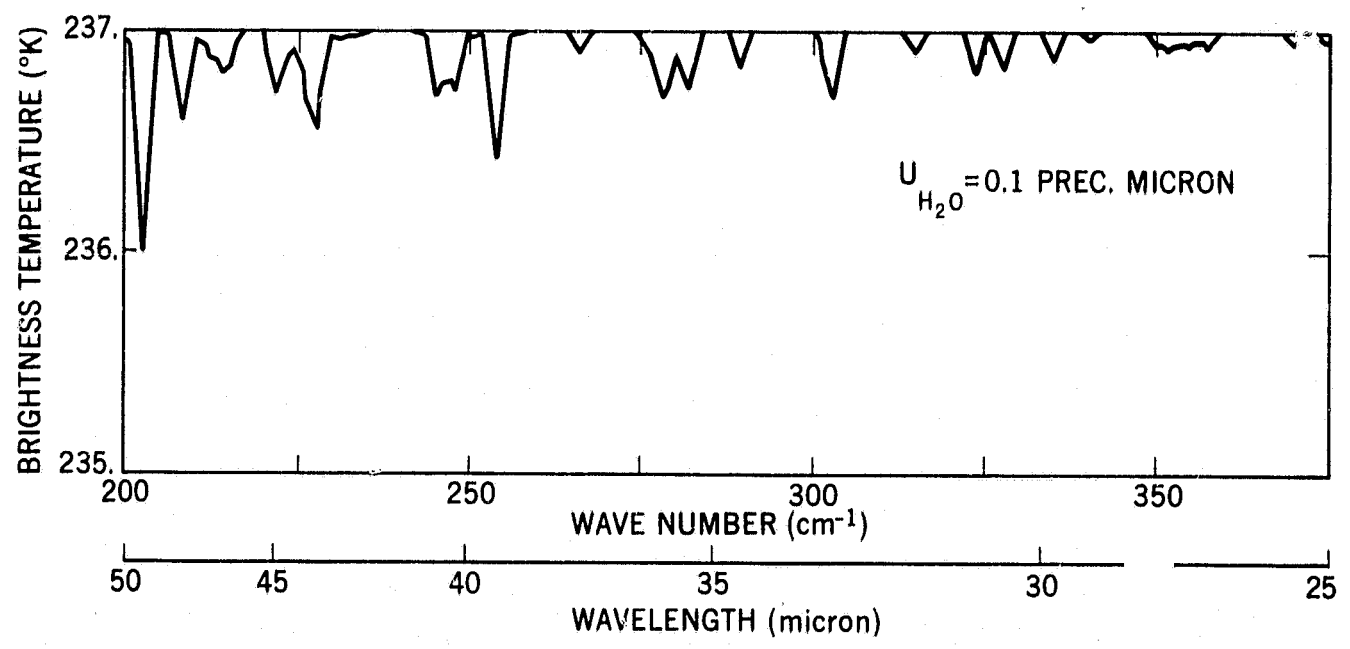

(b)

Figure 5. Synthetic brightness temperature spectra for the rotational lines of water vapor. (a) Spectra calculated assuming water vapor contents of 14.6 precipitable microns and 0.1 precipitable micron with a boundary layer temperature "discontinuity" of 36 °K. (b) Spectrum calculated for 0.1 precipitable micron water vapor content without the boundary layer temperature "discontinuity".

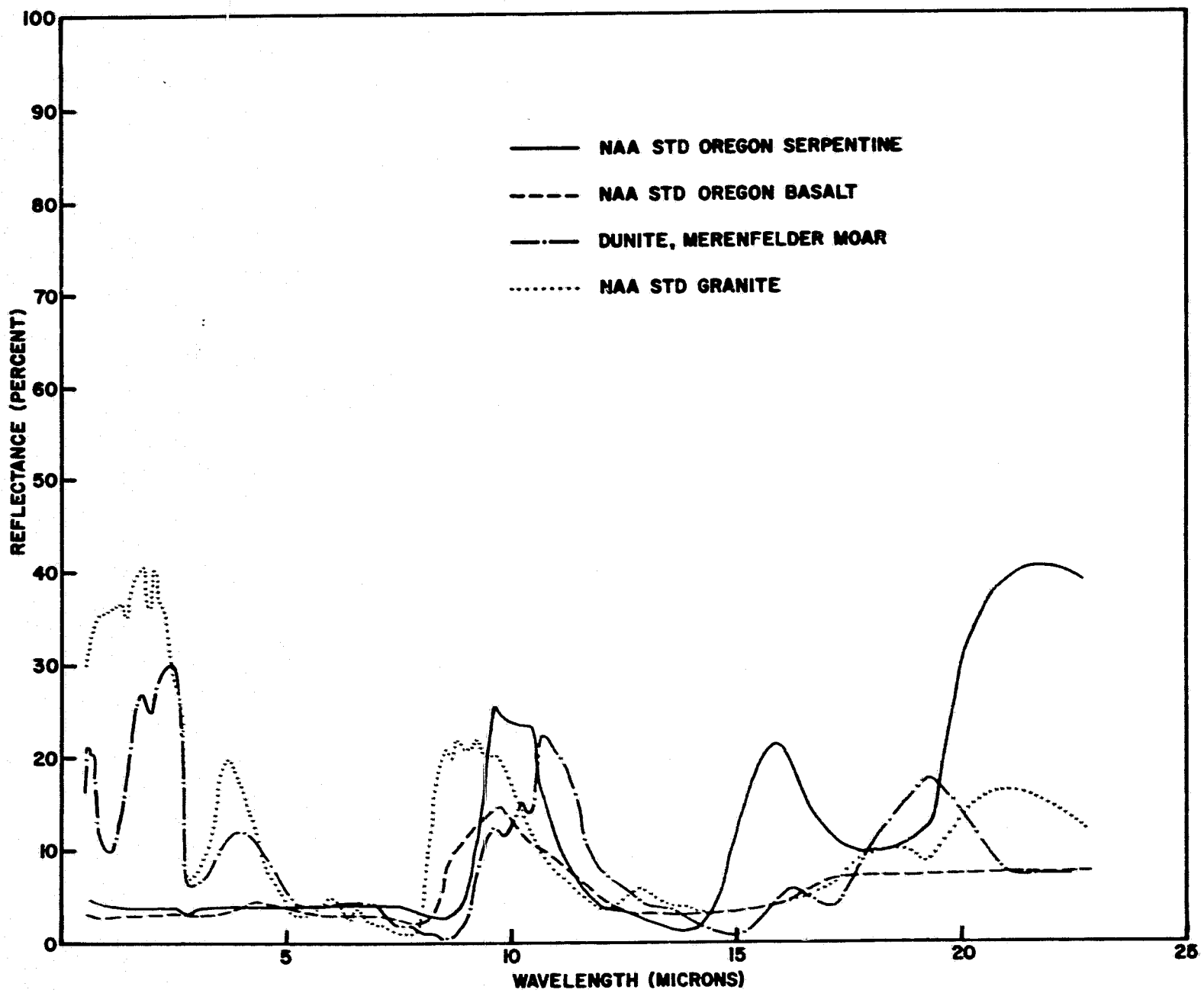

Figure 6. Measured reflectance spectra of solid fractured rock samples displaying the phenomenon of reststrahlen.

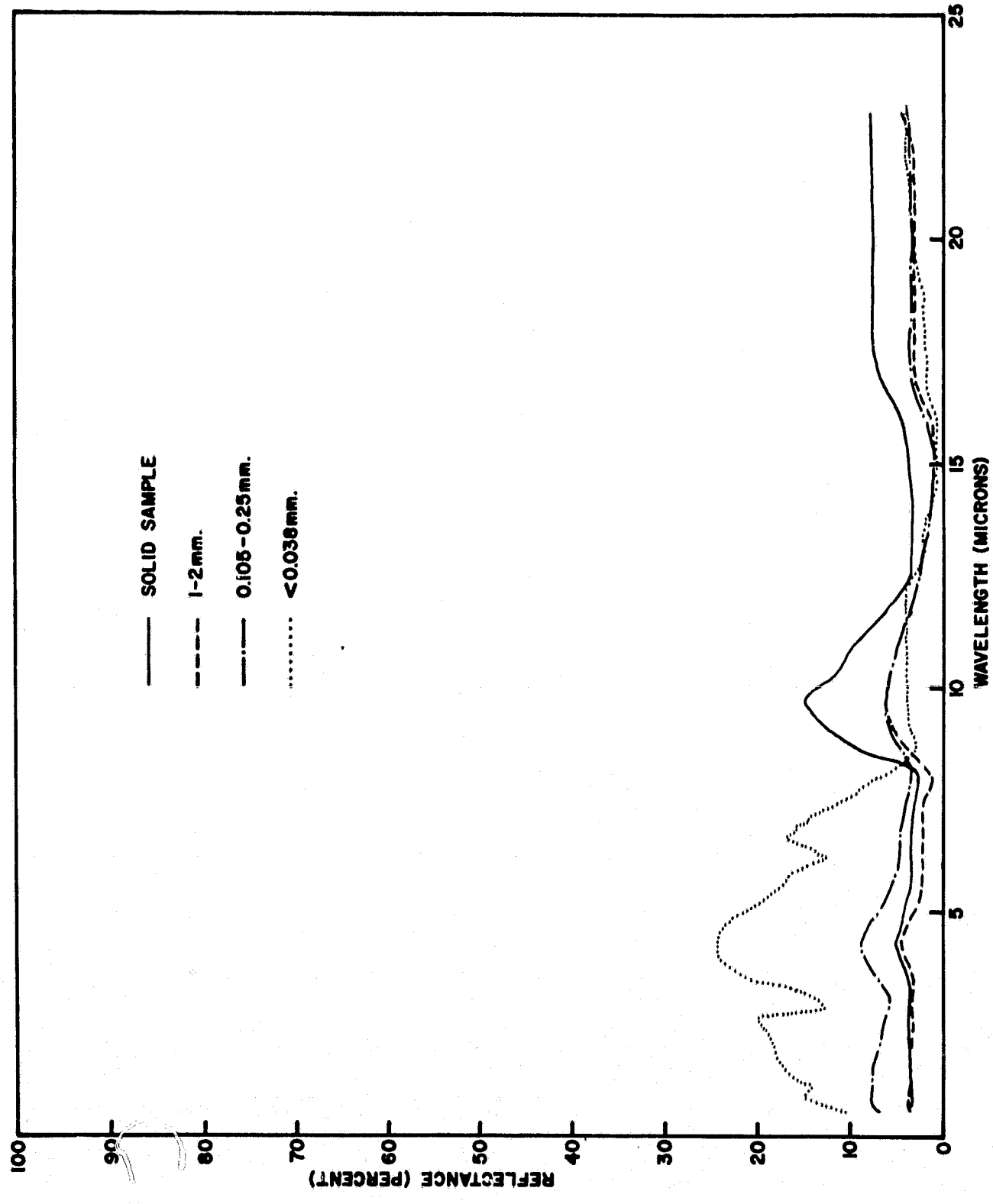

Figure 7. Measured reflectance spectra of solid and ground basalt. The weakening of the reststrahlen features as the material is ground to smaller sizes is illustrated.

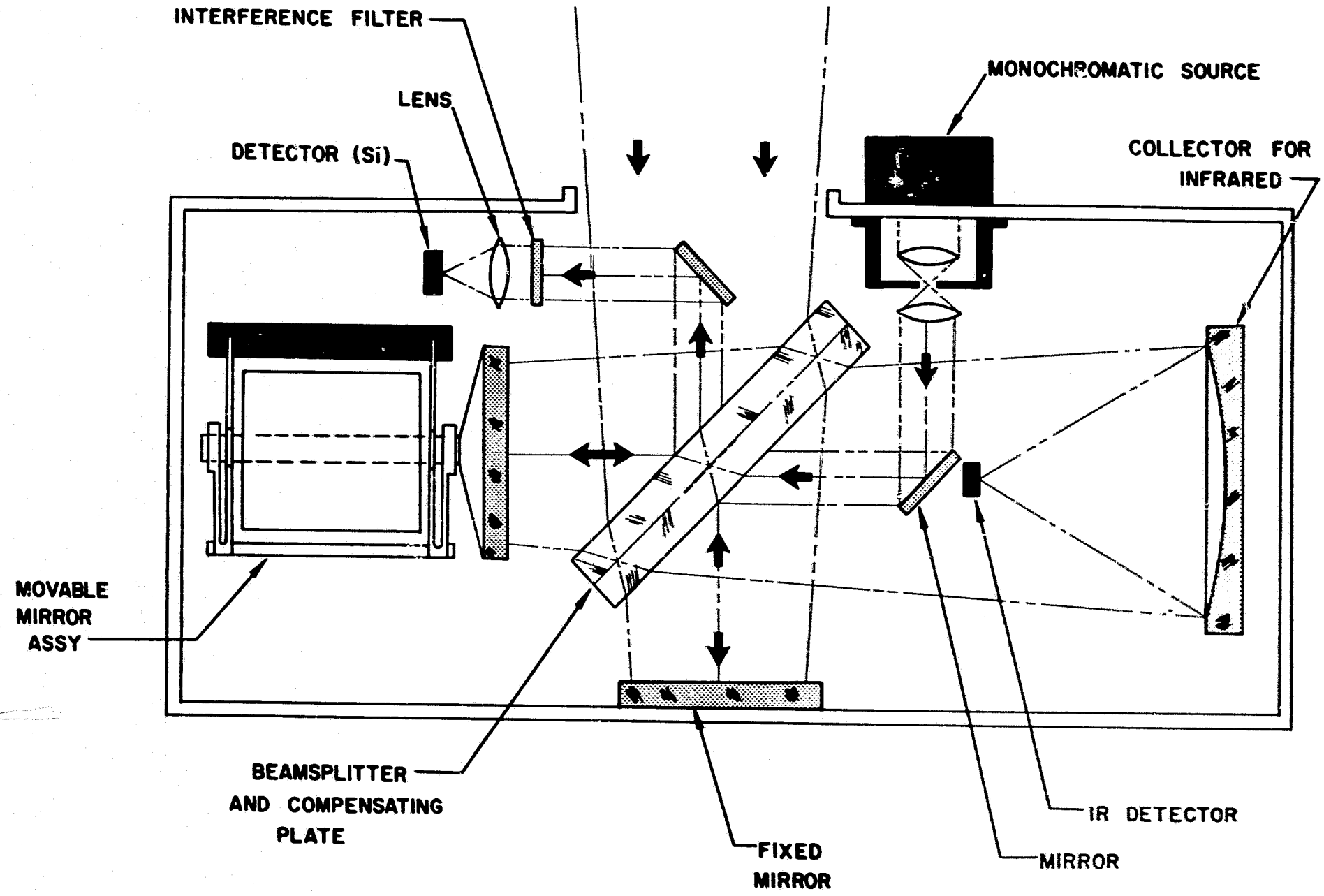

Figure 8. Simplified diagram of Michelson-type interferometer. The reference source is a near infrared line of a neon discharge tube.

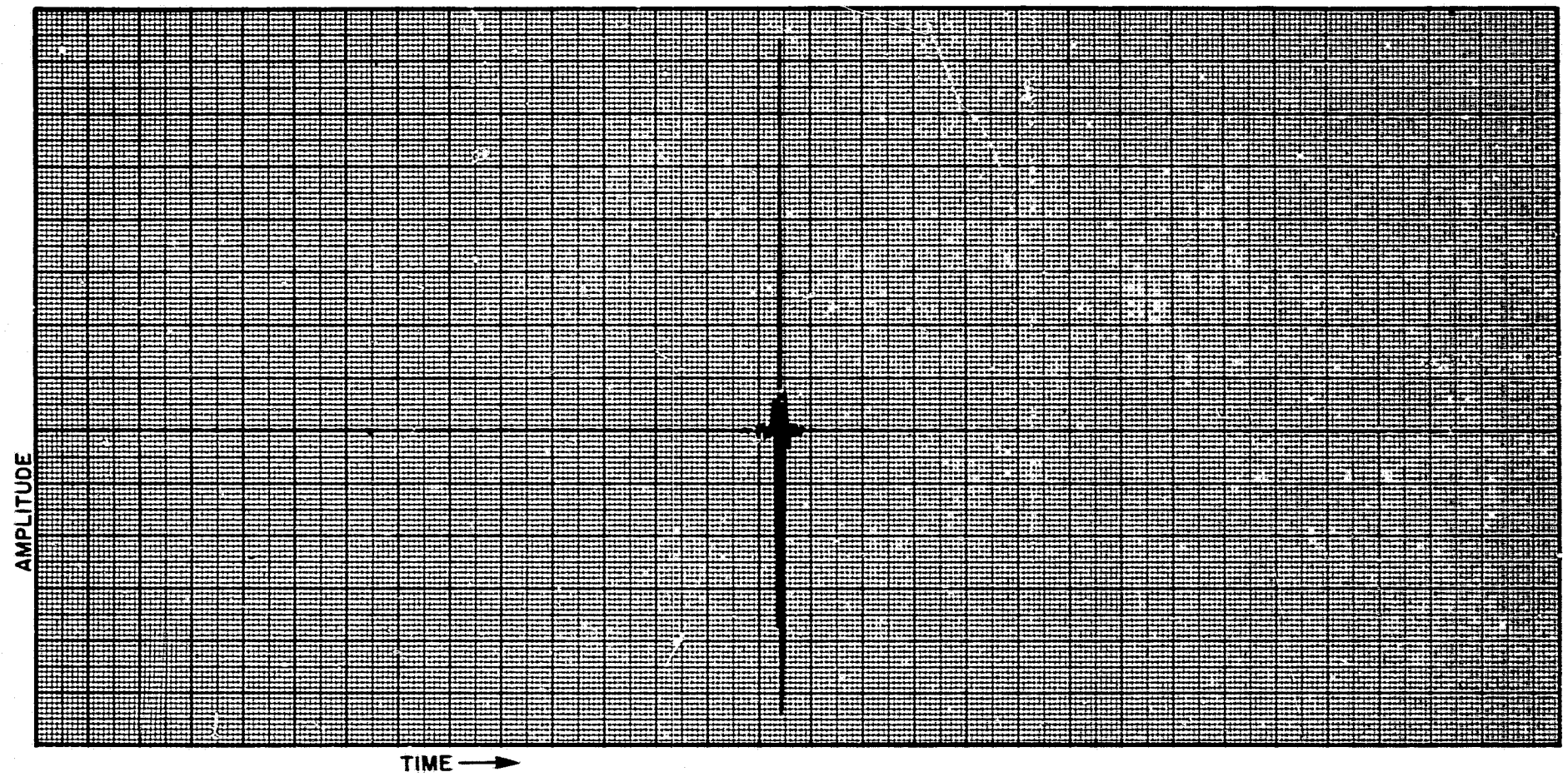

Figure 9. Typical interferogram of a cold blackbody obtained in thermal vacuum chamber with Nimbus B interferometer.

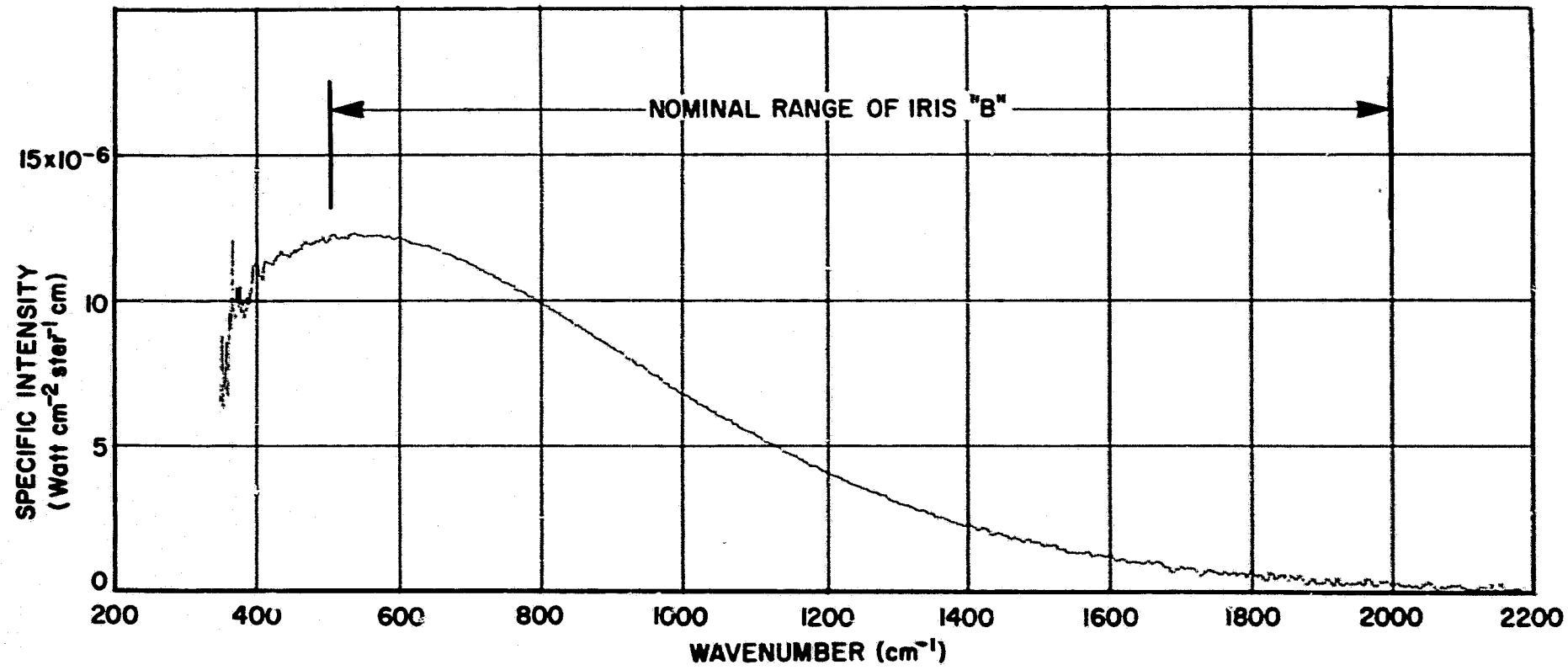

Figure 10. Spectrum derived during thermal vacuum tests of the IRIS-B instrument. The target was a blackbody with a temperature of about 279 °K. The spectrum was computed from a single interferogram such as shown in Figure 9.